Thermal Management of an Avionics Module Using Solid–Liquid Phase-Change Materials

Debabrata Pal*

Motorola Inc., Arlington Heights, Illinois 60004

and

Yogendra K. Joshi†

University of Maryland, College Park, Maryland 20742

A combined experimental and computational investigation of transient thermal control of an avionics module using phase-change material (PCM) is reported. The configuration examined was a honeycomb core filled with an organic PCM, *n*-triacontane, heated from the bottom. Experiments were conducted to evaluate the thermal performance of the PCM device by measuring temperatures at various locations as functions of time until the module temperature reached an acceptable maximum limit. An analysis of melting inside a single honeycomb cell, considering effects of natural convection, showed that, for the power levels and the cell geometry considered, the effect of natural convection on melting was negligible. A system-level analysis of the PCM-filled device followed. Timewise variations of temperatures at various locations from the model were in good agreement with the experimental data. Times for complete melting, maximum temperature variations within the honeycomb, and evolution of melt shapes are presented as functions of power levels.

Nomenclature

b = constant in the porosity source term
C = morphological constant, 1×10^9
c_p = specific heat, J/kg-K
D = sides of the heater, m
d = thickness of Styrofoam® insulation, m
Fo = Fourier number, $\alpha t/l^2$
g = gravitational acceleration, m/s^2
h = heat transfer coefficient, W/m^2-K
k = thermal conductivity, W/m-K
L = latent heat of fusion, J/kg
l = PCM layer thickness, m
p = pressure, N/m^2
Q = total power dissipation, W
Q''' = volumetric heat generation rate, W/m^3
q'' = heat flux, W/m^2
Ra = Rayleigh number, $g\beta_p \Delta T l^3/\alpha_p \nu_p$
S = source term
Ste = Stefan number, $c_{pp} Q l/k_p D^2 L$
T = temperature, °C
u = velocity in x direction, m/s
v = velocity in y direction, m/s
w = velocity in z direction, m/s
α = thermal diffusivity, m^2/s
β = coefficient of volumetric expansion, 1/K
ΔH = latent heat component of enthalpy, J/kg
θ = dimensionless temperature, $[kD^2(T - T_i)/Ql]$
μ = dynamic viscosity, kg-m/s
ρ = density, kg/m^3
τ = dimensionless time, Fo

Subscripts
H = enthalpy
m = melting point
p = phase-change material
0 = ambient

I. Introduction

SOLID–LIQUID phase-change materials (PCMs) have been employed in a wide range of applications including spacecraft thermal management and solar energy storage. Thermal energy storage is achieved as the PCM undergoes a solid-to-liquid phase transition. This type of energy storage can be used for thermal control in situations where heat dissipation is of a periodic nature or a sudden transient. As an application in the latter category, PCM can be used as a passive backup cooling scheme for some duration of time for actively cooled electronics following a cooling system failure. The present study investigates passive thermal control of standard electronic modules (SEM), which are often used in avionics applications. Such modules house the increasingly complex electronics currently employed for various aircraft control purposes. These modules are typically cooled by circulating air or liquid through internally finned passages. For a failure in the active cooling scheme, PCMs offer a passive technique for heat removal for limited times (Fig. 1a). Such backup cooling may avert a catastrophic failure in electronics functions by allowing a safe return to ground.

The following provides a summary of studies involving the use of organic PCMs for various types of thermal control applications. These studies can be divided into three categories. The first category does not consider any metallic filler.[1,2]

In the studies by Humphries and Griggs,[3] Witzman et al.,[4] and Snyder,[5] the effect of using flat fins for thermal enhancement was examined. Henze and Humphrey[6] presented an experimental and numerical study of a finned thermal capacitor. Eftekhar et al.[7] carried out an experimental study of thermal storage using paraffin wax in a finned compartment. Snyder[5] also modeled a finned PCM unit by using effective thermophysical properties and neglecting natural convection.

*Senior Mechanical Engineer, Advanced Products Division, Cellular Infrastructure Group, 1475 West Shure Drive, M/S 3G6.

†Associate Professor, CALCE (Computer Aided Life Cycle Engineering) Electronic Packaging Research Center, Department of Mechanical Engineering.
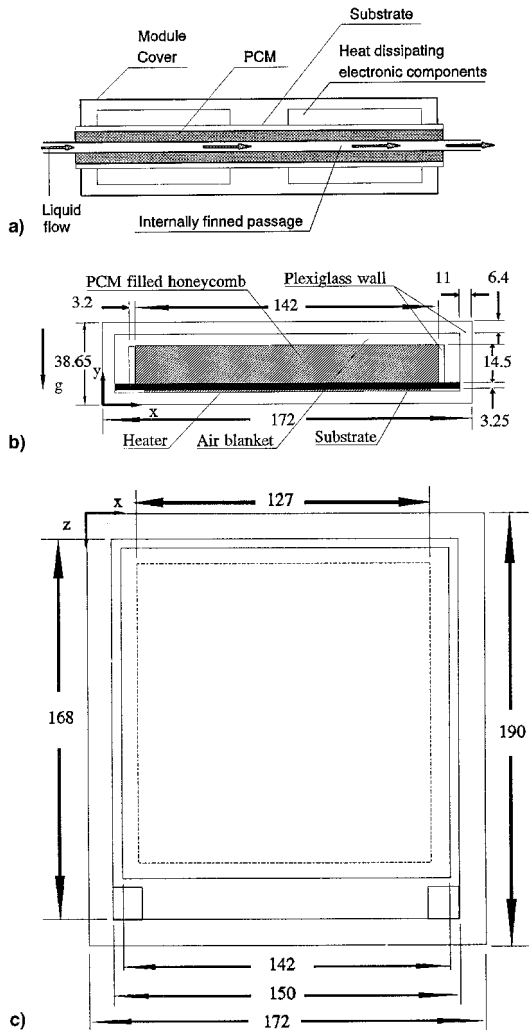
Fig. 1 a) SEM-E module with possible PCM cooling arrangement, b) vertical cross section of the experimental cell, and c) horizontal cross section of the experiment cell (dimensions are in mm).

Incorporation of organic PCM in expanded honeycomb materials has also been used as a technique of thermal performance enhancement. This configuration allows a larger aluminum surface area in contact with the PCM. Abhat[8] performed a combined experimental and computational study of a thermal control unit, where PCM was incorporated in hexagonal honeycomb cells aligned parallel to the heating surface. A simplified thermal network model of a unit cell was developed. Bledjian et al.[9] used an organic PCM in honeycomb in a cylindrical configuration. Duffy[10] used PCM-filled honeycomb for thermal control of an electronic enclosure. Brennen and Suelau[11] experimentally investigated partially and fully expanded honeycombs filled with organic paraffin for thermal control.

The aim of the present paper is to investigate melting of PCM inside honeycomb cores mounted such that the cells are in a vertical orientation. Numerical simulation is done in a single cell, considering the effect of natural convection. The single-cell model showed that the effect of natural convection on melting was very small for the power levels considered. This model was unable to predict the thermal performance of the entire PCM device and was in substantial difference with the experimental data because of neglect of the conjugate heat transfer effects. Therefore, a system-level melting simulation was undertaken, considering the PCM–honeycomb to be an isotropic composite, and results were in good agreement with the experimental data.

II. Experimental Configuration

The configuration studied here (Figs. 1b and 1c) consisted of a horizontal aluminum substrate representative of a commonly used avionics card with a silicone rubber patch heater mounted on the bottom. On the top of the substrate a 14.5-mm-deep honeycomb core was mounted (Fig. 2a) and filled with the organic PCM n-triacontane. Thermophysical data for this PCM are shown in Table 1. To contain the molten PCM, the honeycomb was enclosed by walls of 3.2-mm-thick Plexiglas® (Fig. 1), which was attached to the aluminum substrate by a conductive epoxy adhesive. This assembly was enclosed inside an outer Plexiglas enclosure. The Plexiglas enclosure was placed inside a Styrofoam box with 38.1-mm-thick walls to further reduce heat loss to the surroundings.

T-type thermocouples were placed at strategic locations within the PCM–honeycomb core, on the heater surfaces, and on the outside walls of the Plexiglas (Fig. 2b). The thermocouple signals were conditioned and multiplexed in a National Instruments (NI) SCXI-1100 signal-conditioning module and were fed to the single channel of an NI AT-MIO-16-L-9 data acquisition card connected to a 486-DX personal computer. The front-end software for the data acquisition system was Labview version 3.1 from NI.

Before the experiments, the honeycomb was carefully filled with molten PCM at a temperature of 95°C. After solidification, this resulted in an approximately 10% ullage space. Experiments were started with all the thermocouples initially at room temperature. Temperature uniformity was within ±0.15°C. Uniform power was applied to the module during the entire experiment. Power was set and was controlled by a variac. Temperatures were recorded by the data acquisition system at intervals of 10 s. The sampling rate was 100 per s, and 1000 samples were taken per thermocouple for each reading. Experiments were continued until the heater temperature rose to 105°C, the highest allowable operating temperature of the adhesives used in the setup. Tests were performed
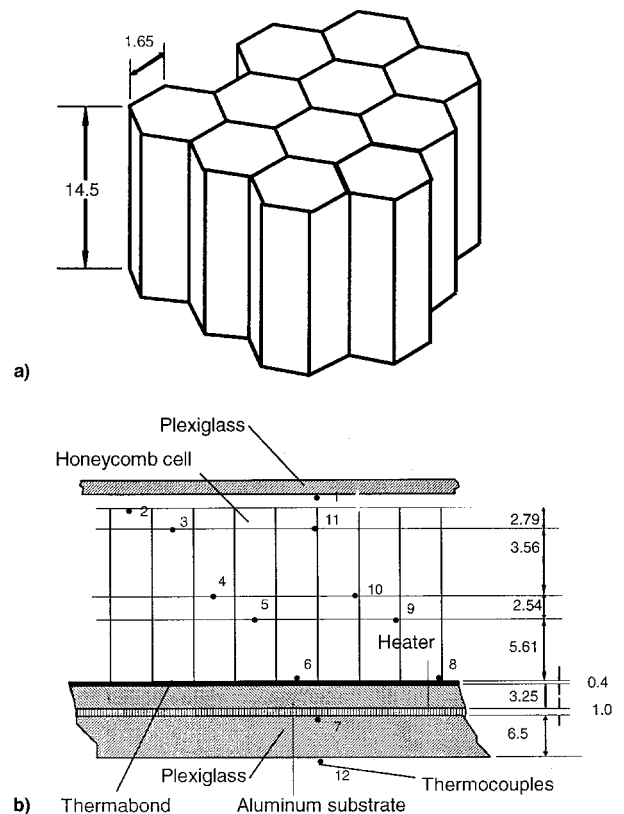

Fig. 2 a) Honeycomb core geometry and b) thermocouple locations (dimensions are in mm).

Table 1 Thermophysical properties used for computation

Materials	k	ρ	c_P	μ
Substrate (aluminum)	204	2707	896	1×10^{30}
Adhesive (epoxy)	1.00	1150	1833	1×10^{30}
Plexiglas	0.19	1180	1255	1×10^{30}
Heater (silicone rubber)	0.23	3970	765	1×10^{30}
RCM (n-triacontane)	0.23	810	2050^a	3.57×10^{-3}

[a]Measured at McDonnell Douglas Corporation. Melting point of PCM: 65.4 deg and latent heat per unit mass: 251 kJ/kg.

over a wide range of power levels, from 15 to 60 W at a step of 5 W.

An ice-bath calibration of the electronic ice-junction-based data acquisition card showed a consistent offset of 0.35°C against a mercury-in-glass thermometer. This difference was subtracted as a correction factor from the temperature measurements. Also, an uncertainty of ±0.15°C was estimated in the temperature measurements based on timewise jitter. Uncertainties in mass and length measurements were ±0.1 g and ±0.5 mm, respectively. Uncertainties for voltage and current measurements were ±0.01 V and ±0.01 A, respectively. Individual uncertainties were combined in the constant odds form at 95% confidence level, using the technique by Kline and McClintock.[12] The resulting uncertainty for power measurement was ±0.327% for a power level of 60 W.

III. Melting Model of PCM in a Single Honeycomb Cell

The experiments considered heating the honeycomb cores from the bottom. For such a configuration, melting is initiated near the aluminum substrate–PCM interface (Fig. 1), and the melt front progresses upward. As a result of gravity, this may set up a convective motion inside the melt pool within a honeycomb cell. This natural convection may add to the conduction heat transfer at the solid–liquid interface and enhance the melting process. Therefore, including the effect of natural convection is necessary if it is important for a particular heating configuration.

The study of natural convection in bottom-heated cell arrays like honeycombs has received considerable research interest in the past. At Rayleigh numbers below the critical level Ra_{crit}, heat transfer occurs by conduction only. Ra_{crit} depends on the cell aspect ratio, cell shape, and fluid thermophysical properties. Sun and Edwards[13] studied natural convection within an array of circular and rectangular cells filled with water, heated from the bottom. The Rayleigh number range considered was $6 \times 10^3 - 10^6$. The aspect ratio range considered was 0.78–4.0. Ra_{crit} was found to increase with an increase in the cell aspect ratio. Catton and Edwards[14] examined natural convection in hexagonal honeycomb cores filled with water and silicone oil. The bottom and the top boundaries were maintained at constant temperature. They presented Ra_{crit} as a function of the aspect ratio for insulating and conducting boundary walls. Cane et al.[15] reported an experimental study of natural convection of air in inclined honeycomb panels for various aspect ratios.

From the experimental data, the Rayleigh number range covered was 368–1470. The aspect ratio of a single cell of honeycomb is roughly 4.75:1. The near-hexagonal cross section of the honeycomb was approximated as a square with the same perimeter. The computational domain is shown in Fig. 3. The cell is heated at the bottom by a uniformly dissipating heater. This domain was discretized in an $18 \times 60 \times 18$ nonuniform grid for all computations. Computations using a refined grid $(22 \times 74 \times 22)$ resulted in a maximum difference of 2% in the maximum temperature. Hence, all computations were done in $18 \times 60 \times 18$ grids.

A. Governing Equations

Assuming the flow of the molten PCM to be Newtonian and laminar, the time-dependent governing equations for mass, en-
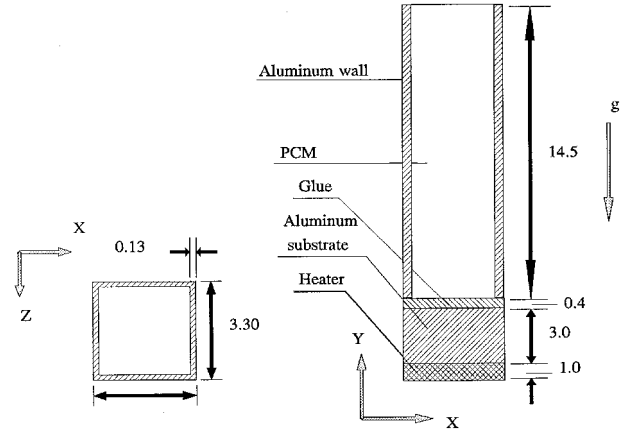

Fig. 3 Computational domain for a single cell (dimensions in mm).

ergy conservation, and force–momentum balance are written in dimensional form.

Continuity:

$$\frac{\partial}{\partial x}(\rho u) + \frac{\partial}{\partial y}(\rho v) + \frac{\partial}{\partial z}(\rho w) = 0 \qquad (1)$$

x momentum:

$$\frac{\partial}{\partial t}(\rho u) + \frac{\partial}{\partial x}(\rho u u) + \frac{\partial}{\partial y}(\rho v u) + \frac{\partial}{\partial z}(\rho w u) = \frac{\partial}{\partial x}\left(\mu \frac{\partial u}{\partial x}\right)$$
$$+ \frac{\partial}{\partial y}\left(\mu \frac{\partial u}{\partial y}\right) + \frac{\partial}{\partial z}\left(\mu \frac{\partial u}{\partial z}\right) - \frac{\partial p}{\partial x} + S_x \qquad (2)$$

y momentum:

$$\frac{\partial}{\partial t}(\rho v) + \frac{\partial}{\partial x}(\rho u v) + \frac{\partial}{\partial y}(\rho v v) + \frac{\partial}{\partial z}(\rho w v)$$
$$= \frac{\partial}{\partial x}\left(\mu \frac{\partial v}{\partial x}\right) + \frac{\partial}{\partial y}\left(\mu \frac{\partial v}{\partial y}\right) + \frac{\partial}{\partial z}\left(\mu \frac{\partial v}{\partial z}\right)$$
$$- \frac{\partial p}{\partial y} + S_y + \rho g \beta (T - T_m) \qquad (3)$$

z momentum:

$$\frac{\partial}{\partial t}(\rho w) + \frac{\partial}{\partial x}(\rho u w) + \frac{\partial}{\partial y}(\rho v w) + \frac{\partial}{\partial z}(\rho w w)$$
$$= \frac{\partial}{\partial x}\left(\mu \frac{\partial w}{\partial x}\right) + \frac{\partial}{\partial y}\left(\mu \frac{\partial w}{\partial y}\right) + \frac{\partial}{\partial z}\left(\mu \frac{\partial w}{\partial z}\right)$$
$$- \frac{\partial p}{\partial z} + S_z \qquad (4)$$

Table 2   Source terms for various materials

	S_x	S_y	S_z	S_h
Air	0	$\rho g \beta (T - T_0)$	0	0
PCM	$\dfrac{C(1-\varepsilon)^2}{\varepsilon^3 + b} u$	$\dfrac{C(1-\varepsilon)^2}{\varepsilon^3 + b} v$	$\dfrac{C(1-\varepsilon)^2}{\varepsilon^3 + b} w$	$-\rho \dfrac{\partial(\Delta H)}{\partial t}$
Heater	0	0	0	Q'''
Other solids	0	0	0	0

Energy:

$$\frac{\partial}{\partial t}(\rho c_p T) + \frac{\partial}{\partial x}(\rho u c_p T) + \frac{\partial}{\partial y}(\rho v c_p T) + \frac{\partial}{\partial z}(\rho w c_p T)$$

$$= \frac{\partial}{\partial x}\left(k\frac{\partial T}{\partial x}\right) + \frac{\partial}{\partial y}\left(k\frac{\partial T}{\partial y}\right) + \frac{\partial}{\partial z}\left(k\frac{\partial T}{\partial z}\right) + S_h \qquad (5)$$

An adiabatic thermal boundary condition was employed for the top and bottom surfaces of the cell. Symmetric, and therefore adiabatic, boundary conditions were imposed on the four sidewalls of the cell. The same sets of equations apply for various materials. The thermophysical properties of various materials are provided in Table 1, and the expressions for coefficients and source terms for various materials used for computations are listed in Table 2.

The modeling of phase change was done using a single-domain enthalpy–porosity technique.[16] The calculation of phase-change interfaces was implicit and did not require an explicit phase-front tracking. Instead, the solid–liquid interface was treated as a numerical mushy zone of porosity ε with a width of one control volume. Control volumes containing only solid have a value of $\varepsilon = 0$, and the ones containing only liquid have a value of $\varepsilon = 1$. According to Brent et al.,[16] to assure convergence, the numerical implementation of the change in velocity from solid to liquid should be based on a method that provides a smooth transition. This is ensured in the present technique by using the notion of the numerical mushy zone.

B.   Numerical Procedure

When solving for a single cell, the governing equations were solved by a finite volume-based procedure using SIMPLER algorithm.[17] Convergence was said to be achieved when the normalized maximum difference in temperature between successive iterations and normalized energy balance residual fell below 1×10^{-5} and 1×10^{-4}, respectively. Selection of a proper time step was required to ensure faster convergence and to yield a time-step-independent solution. This was tested by using various time steps and, based on these results, a time step of 5 s was chosen. However, for the simulations considering effects of convection, a further reduction of time steps to 2 s was necessary.

Validation of the code was done by solving the problem of melting of gallium in a two-dimensional cavity.[16] The locations of melt fronts at various times compared within 1.0% of their solution.

C.   Computations for Melting in a Single Cell

Illustrative results are presented in Fig. 4 for a module power of 60 W, which corresponds to the highest level employed in the experiments. Two different computations were done; the first one was without the effects of natural convection, and in the second one natural convection was modeled. Figure 4 presents the velocity vectors and the isotherms for these two cases at a vertical section through the midplane ($z = 1.65$ mm). The comparison between the melt shapes at various times shows that, although there is a weak natural convection flow, it is not affecting the melt shape noticeably. As time progresses, the melt thickness along the walls increases and reaches the top of the honeycomb (Fig. 4a). The melt layer
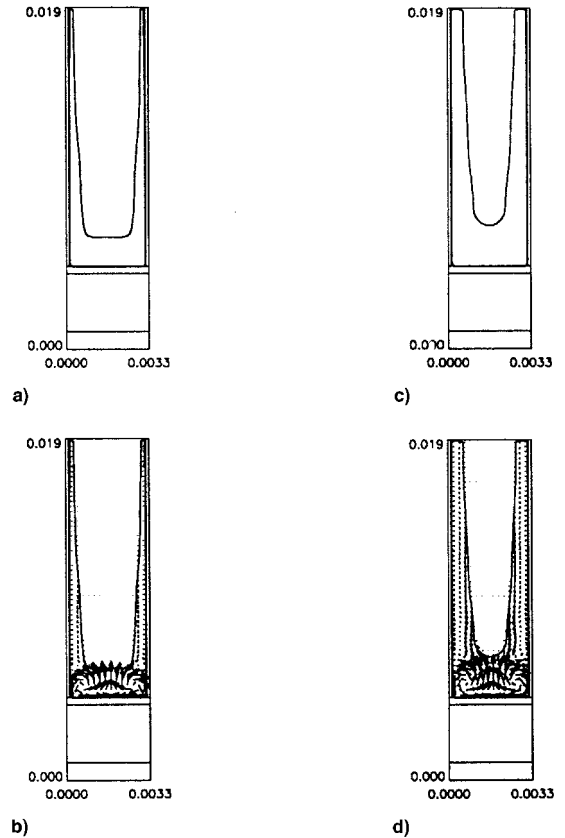

Fig. 4   Melt shapes for cases with and without natural convection at the vertical midplane ($z = 1.65$ mm) for a power level of 60 W. Maximum velocity magnitude is 0.19 mm/s: a) 400, b) 400, c) 600, and d) 600 s.

thickness along the bottom surface also increases, and finally the layers merge and grow. During early melting ($t = 400$ s), the molten PCM rises as an upward plume. This plume impinges on the solid–liquid interface and comes down along the edges of the honeycomb walls, producing two counter-rotating cells. Later, hot and molten PCM rises along the honeycomb wall, transfers heat, and comes down along the solid–liquid interface. This leads to another set of counter-rotating cells near the top left and right (Fig. 4c). The maximum velocity magnitude for this simulation was only about 0.19 mm/s. Another simulation was performed to study the effect of the conducting sidewalls on the natural convection. The maximum velocity magnitude for the case with sidewalls replaced by adiabatic walls showed an increase by a factor of 10, with other conditions remaining the same. This corroborates the observation by Catton and Edwards[14] that the presence of conducting sidewalls acts to dissipate temperature perturbations and therefore suppress the natural convection.

Figure 5 compares the single-cell data with the experimental data. The timewise variation of the temperature at the bottom of the honeycomb is plotted as a function of time. The difference is mainly caused by the absence of heat loss to the surroundings and conjugate heat transfer effects from the heater to the Plexiglas by conduction. In the presence of discrete heat-
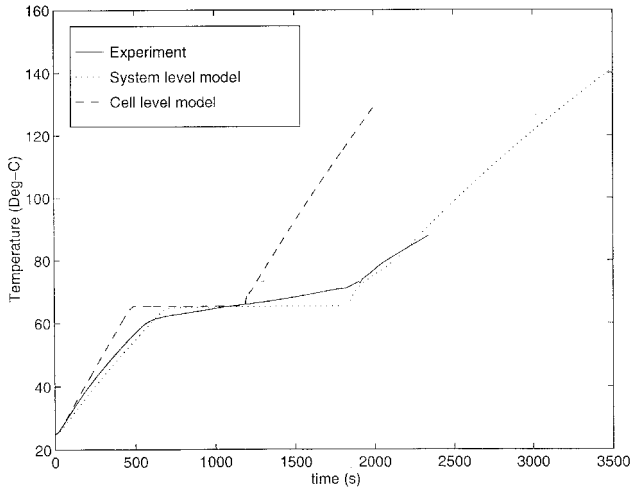
Fig. 5   Timewise variation of temperature for experiment, system-level model, and single-cell model. Power level = 60 W.

ing, the conduction into the substrate near the heater ends cannot be treated by a unit-cell-type analysis. This suggests the use of a conjugate system-level analysis for the PCM device, accounting accurately for the heat losses to the surrounding solid regions. This model, described in the following text, resulted in the significantly improved comparison with the data reported in Fig. 5.

IV.   System-Level Model for Melting Within Honeycomb

The entire avionics card assembly, with the heater, PCM–honeycomb composite, and the outer Plexiglas enclosure was modeled. The results from the melting analysis inside a single honeycomb cell in Sec. III justified the use of a conduction-driven melting global model, because the effect of natural convection on melting was negligible. The PCM–honeycomb composite was assumed homogenous and isotropic, the PCM and neighboring honeycomb were in local thermal equilibrium, and thermophysical properties were independent of temperature.

For a volume element containing honeycomb and solid and liquid PCM, the volume fraction of PCM is defined as $\delta = V_{Al}/V$, where V_{Al} is the volume occupied by the aluminum, and V is the total volume. The value of δ used was 0.025, as measured.

The effective thermal capacitance and the effective thermal conductivity were expressed as

$$\overline{\rho c} = \rho_{PCM} C_{PCM} (1 - \delta) + \rho_{Al} C_{Al} \delta \qquad (6)$$

The effective thermal conductivity depends on the structure of the composite. Assuming a parallel path of heat conduction through the PCM and the honeycomb walls, this is defined as

$$k_{eff} = (1 - \delta) k_{PCM} + \delta k_{Al} \qquad (7)$$

Computations were done in three dimensions. A nonuniform $24 \times 21 \times 26$ grid was used. For grid refinement, computations were done for a power level of 15 W on a $26 \times 72 \times 28$ grid. A maximum difference in maximum temperature was less than 2%, and the coarser grid was chosen for all of the computations. The heater was assumed to have uniform volumetric heat generation and uniform thermophysical properties. The heat loss through the Styrofoam walls was modeled with a variable heat flux boundary condition at all the Plexiglas surfaces. The variable heat flux at a wall is determined by using a one-dimensional thermal resistance model. That is, q on a wall is given by

$$q = -\frac{k_i (T_{av} - T_o)}{d} \qquad (8)$$

where k_i is the thermal conductivity of the insulation and T_{av} is the average temperature on the outer surface of Plexiglas walls. T_o was 25°C for all experiments. The heat fluxes on each of the six walls were updated after each computational cycle for one time step.

V.   Measurements and Comparison with System-Level Model

Figure 6 shows the timewise variation of the temperature at three different locations within the honeycomb for a power dissipation of 30 W. Three distinct stages can be observed for each curve. Initially, the PCM is heated from the ambient temperature to its melting point, which is the premelt stage. This is followed by the second stage, when the PCM undergoes phase change and the temperatures at the top and the bottom of the PCM are stabilized at the melting temperature. Because of the existing thermal resistance from the heater to the PCM, the heater temperature shows a larger temporal variation during the phase change. Following the completion of melting, in the third stage, sensible heating causes the temperatures to increase. The computations for the PCM temperatures generally matched well with the experiments.

The differences in the honeycomb temperatures (top and bottom) between the model and the test data during melting were within 7%. These could be a result of the possible non-isothermal phase-change behavior of the paraffin n-triacontane. Differential scanning calorimetry data to measure the melting point and the latent heat showed a melting temperature range of ±3°C around the melting point, which was 65.4°C. In the model, a constant melting temperature of 65.4°C was chosen. The same can be attributed to the difference in the melting times predicted by the model and experimental data, for which a maximum difference of 3% was observed.

A maximum of 13% difference between the experimental data and computational prediction is observed in Fig. 6 for the heater surface (facing down on the Plexiglas) temperature for this power level. This difference is attributed mainly to the contact thermal resistance existing between the heater and the aluminum substrate in the experiment and to the assumption that the heater is uniformly dissipating. This difference was found to vary between 10% for a power level of 15 W and 18% for a power level of 60 W. Following the melting, during the second sensible heating period, the slopes of experimental measurements were somewhat lower than the computational results. This is possibly from the approximate heat-loss model implemented in computations.
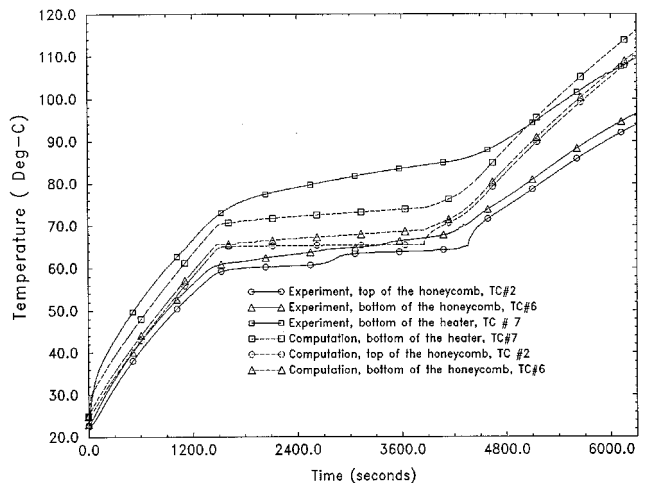

Fig. 6   Timewise variation of PCM top, bottom, and heater temperatures. Power level = 30 W.

An appropriate combination of dimensionless parameters is needed for useful data reduction. The characteristic length was chosen to be l. The nondimensional power levels were expressed by the Stefan number as

$$Ste = c_p Ql/kD^2L \qquad (9)$$

Dimensionless time τ was chosen as Fo, which is given by

$$Fo = \alpha t/l^2 \qquad (10)$$

The dimensionless temperature θ is given by

$$\theta = (kD^2/Ql)(T - T_i) \qquad (11)$$

The maximum uncertainties in Fo, Ste, and θ were found to be ±6.9, ±3.4, and $\pm3.5\%$, respectively.

Figure 7 shows the computational results of the melt fraction vs $Ste.Fo$ for various power levels. The initiation of melting was chosen as $Ste.Fo = 0$. This plot shows that the melting rates were almost linear with $Ste.Fo$, except during the beginning and completion of the melting.

Experiments were also done by filling the honeycomb core to a height of 7.25 mm, which is approximately 50% of the honeycomb core height. Figure 8 compares the time required for complete melting, as a function of Ste, for two different PCM thicknesses. Based on this plot, it was found that the data for two different thicknesses follow the same curve. This indicated that l is the proper choice for characteristic length.
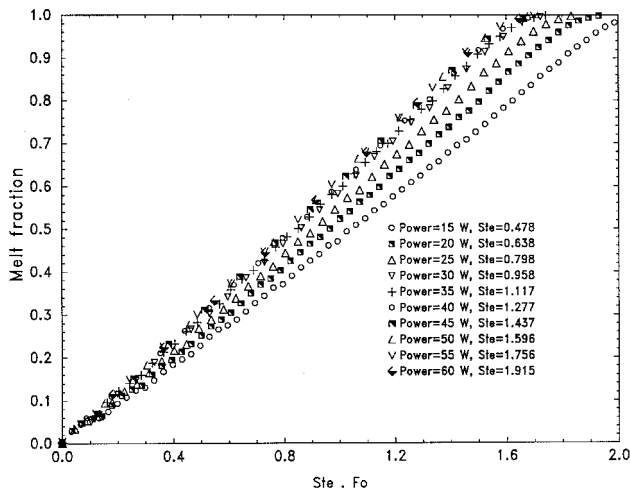
Good agreement was found between the experimental and computational results.

The temperature differential within the PCM device is an extremely important application parameter. This is a strong function of the effective thermal conductivity of the PCM–honeycomb composite, and the orientation of the medium, in the presence of natural convection. The maximum temperature differential across the honeycomb occurs at the completion of melting. An increase in power level results in higher temperature nonuniformities inside the PCM–honeycomb core (Fig. 9). Comparison with the data from Abhat[8] showed no significant difference in performance between the horizontal and the vertical orientation of the honeycomb core.

The melt shapes and isotherms through the vertical section across the midplane ($z = 0.095$ m) are plotted in Fig. 10 for a power level of 30 W. The melt shape was horizontal except at the edges, where additional heat losses exist. Isotherms in Fig. 10 showed large gradients near the Plexiglas walls.

Figure 11 shows the heat transfer contributions through various boundaries at the completion of melting. It can be ob-

Fig. 7   Melting rates for various power levels.
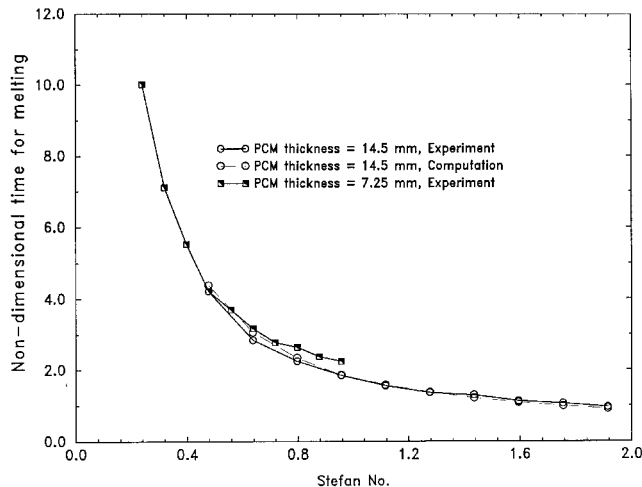
Fig. 8   Time for complete melting for various power levels.
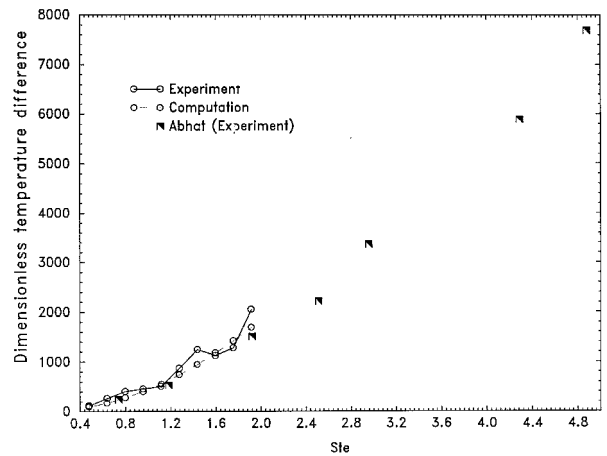

Fig. 9   Maximum temperature variation within the honeycomb for various power levels.
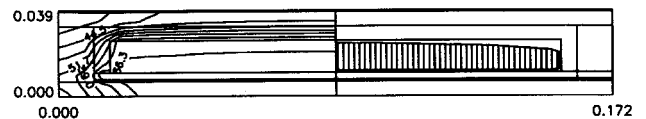

Fig. 10   Isotherms (left half of figure) and melt shapes (right half of figure) for the PCM–honeycomb composite for a power level of 30 W at $z = 0.095$ m; $t = 3500$ s.
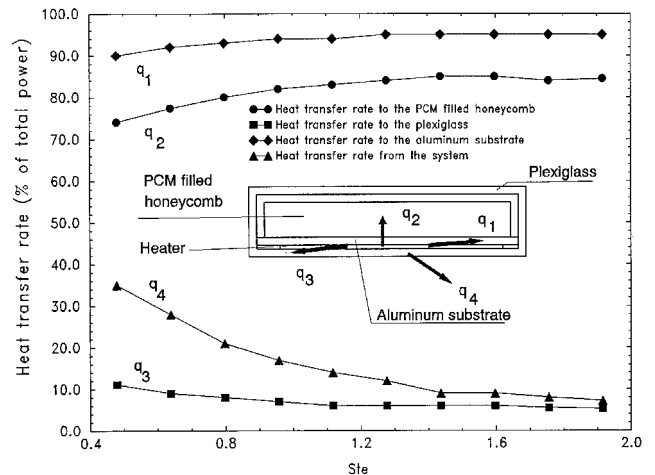

Fig. 11   Energy transfer budget for the system-level analyses. Heat transfer rates shown are at the time of completion of melting.

served that, from the heater, about 90% of the heat transfer takes place to the aluminum substrate and only 10% to the Plexiglas, and no significant variation is observed over the power levels considered. Heat transfer to the honeycomb–PCM from the aluminum substrate is between 74 and 84% over the power level of 15 and 60 W. Heat loss from the system was found to vary between 32% for 15 W and 8% for 60 W. This is because for the lower power levels the preheat time was larger, which caused a higher rate of heat leakage to the surroundings.

VI. Conclusions

Based on the computations and experiments described in the preceding text, the following conclusions can be drawn:

1. The effect of natural convection on melting inside single honeycomb cells was found negligible for the heat fluxes considered, mainly from the presence of conducting sidewalls. With adiabatic sidewalls, the maximum velocity magnitude was found to increase by a factor of 10.

2. A single-cell model of melting is not sufficient for accurate prediction of thermal performance of the system, because it does not consider the heat losses and conjugate nature of transport appropriately. Figure 4 suggests that the prediction of melting time for the single-cell model is in error by more than 50% compared to the experiment.

3. In appropriate normalized form, the melting rate was linear with time. With the choice of $Ste.Fo$ as the time scale and l as the length scale, the melting rates collapsed within a narrow band.

4. In an actual application of thermal control of avionics using phase-change materials, using a device similar to that studied in this paper, the design procedure will be independent of the orientation of the device, because the heat transfer is dominated by conduction, and the effect of natural convection on melting of PCM in honeycomb cells is negligible.

Acknowledgments

References

[1]Pujado, P. R., Stermole, F. J., and Golden, M. O., "Melting of a Paraffin Slab as Applied to Phase-Change Thermal Control," *Journal of Spacecraft and Rockets*, Vol. 6, 1969, pp. 280–284.

[2]Chebi, R., Rice, P. A., and Schwarz, J. A., "Heat Dissipation in Microelectronic Systems Using Phase Change Materials with Natural Convection," *Chemical Engineering Communication*, Vol. 69, 1988, pp. 1–12.

[3]Humphries, W. R., and Griggs, E. L., "A Design Handbook of Phase Change Thermal Control and Energy Storage Devices," NASA TP 1074, 1974.

[4]Witzman, S., Shitzer, A., and Zvirin, Y., "Simplified Calculation Procedure of a Latent Heat Reservoir for Stabilizing the Temperature of Electronic Devices," *Proceedings of the Winter Annual Meeting of the ASME*, edited by S. Oktay, et al., Heat Transfer Div., Vol. 28, American Society of Mechanical Engineers, Boston, MA, 1983, pp. 29–34.

[5]Snyder, K. W., "An Investigation of Using a Phase-Change Material to Improve the Heat Transfer in a Small Electronic Module for an Airborne Radar Application," *Proceedings of the International Electronics Packaging Conference*, Vol. 1, 1991, pp. 276–303.

[6]Henze, R. H., and Humphrey, J. A. C., "Enhanced Heat Conduction in Phase-Change Thermal Energy Storage Devices," *International Journal of Heat and Mass Transfer*, Vol. 24, 1981, pp. 459–472.

[7]Eftekhar, J., Haji-Sheikh, A., and Lou, D. Y. S., "Heat Transfer Enhancement in a Paraffin Wax Thermal Storage System," *Journal of Solar Engineering*, Vol. 106, 1984, pp. 299–306.

[8]Abhat, A., "Experimental Investigation and Analysis of a Honeycomb-Packed Phase Change Material Device," AIAA Paper 76-437, 1976.

[9]Bledjian, L., Burden, J. R., and Hanna, W. H., *Development of a Low-Temperature Phase Change Thermal Capacitor*, edited by R. Viskanta, Vol. 65, Progress in Astronautics and Aeronautics, AIAA, New York, 1979, pp. 255–274.

[10]Duffy, V., "Thermal Control Through Fusible Materials," *Electronic Packaging and Production*, July 1970, pp. 45–53.

[11]Brennen, P. J., and Suelau, H. J., *Low-Temperature Phase-Change Material Package*, edited by L. S. Fletcher, Vol. 60, Progress in Astronautics and Aeronautics, AIAA, New York, 1978, pp. 371–381.

[12]Kline, S. J., and McClintock, F. A., "Describing Uncertainties in Single-Sample Experiments," *Mechanical Engineering*, Vol. 75, Jan. 1953, pp. 3–8.

[13]Sun, W. M., and Edwards, D. K., "Natural Convection in Cells with Finite Conducting Side Walls Heated from Below," *Heat Transfer 1970, Proceedings of the 4th International Conference* (Versailles, France), 1970.

[14]Catton, I., and Edwards, D. K., "Effect of Side Walls on Natural Convection Between Horizontal Plates Heated from Below," *Journal of Heat Transfer*, 1967, pp. 295–299.

[15]Cane, R. L. D., Hollands, K. G. T., Raithby, G. D., and Unny, T. E., "Free Convection Heat Transfer Across Inclined Honeycomb Panels," *Journal of Heat Transfer*, 1977, pp. 86–91.

[16]Brent, A. D., Voller, V. R., and Reid, K. J., "Enthalpy–Porosity Technique for Modeling Convection–Diffusion Phase Change: Application to the Melting of a Pure Metal," *Numerical Heat Transfer*, Vol. 13, 1988, pp. 297–318.

[17]Patankar, S., *Numerical Heat Transfer and Fluid Flow*, Hemisphere, Washington, DC, 1980.